4-17-2020

Assembly of the Photosystem II Reaction Center

Annaliesa Renee Fanguy

Assembly of the Photosystem II Reaction Center

by

Annaliesa Renee Fanguy

Undergraduate honors thesis under the direction of

Dr. David Vinyard

Department of Biological Sciences

Submitted to the LSU Roger Hadfield Ogden Honors College in partial fulfillment of the Upper Division Honors Program.

April 17, 2020

Louisiana State University
& Agricultural and Mechanical College
Baton Rouge, Louisiana

Abstract

In cyanobacteria, algae, and plants, Photosystem II (PSII) is localized to the thylakoid membrane and uses sunlight to oxidize water to molecular oxygen. The active site of water oxidation is the oxygen-evolving complex (OEC), a Mn_4CaO_5 cluster embedded in the PSII protein matrix. In this thesis, we aimed to understand how the OEC can be depleted and reconstituted, and how PSII protein subunits assemble.

The OEC is photo-assembled from Mn^{2+}, Ca^{2+}, and water. To study this process in vitro, PSII membranes are isolated, depleted of the native OEC, then placed under conditions where the OEC can be reformed. However, steps used to deplete the OEC also affect binding of the extrinsic subunits PsbO, PsbP, and PsbQ. Many methods for removing these extrinsic proteins and depleting the OEC have been outlined in literature. We set out to characterize these protocols. We found that treatment of spinach PSII membranes with $CaCl_2$ and NH_2OH removes all of the extrinsic proteins as well as most of the Mn. PSII membranes treated with NaCl and NH_2OH were depleted of Mn and lacked the extrinsic subunits PsbP and PsbQ, but PsbO was still present. Samples treated with only NH_2OH lacked PsbP and PsbQ, but still contained some Mn. Finally, after an alkaline shock treatment, the PSII membranes contained PsbO as well as most of Mn.

During assembly of the PSII complex in cyanobacteria, proteins are trafficked from the plasma membrane to the thylakoid membrane. The tetratricopeptide repeat protein PratA is localized to the intersection of these membrane systems and plays an unknown role in the efficient assembly of PSII. We have heterologously expressed PratA from the cyanobacterium *Synechocystis* sp. PCC 6803 in *E. coli*. We did not observe any interactions between recombinant PratA and PSII membranes. Using mass spectrometry, we found that the Hsp70 homologs DnaK1 and DnaK2 bind to PratA in vitro. This observation led to the hypothesis that PratA recruits chaperones to membrane intersections to facilitate efficient relocation of PSII intermediates.

Acknowledgments

These projects could not have been done without the support, motivation, and encouragement of some very important people:

I would, first and foremost, be remiss if I did not express my deepest gratitude to Dr. David Vinyard for allowing me to take part in his research and for his earnest mentorship over the past four years. I have learned a lot through my experiences in the laboratory, not only about science but also about myself.

Dr. Syed Lal Badshah, thank you for assisting me with running necessary experiments while I was away from the lab due to classes.

To Maria “Rita” Riggio, thank you for always helping me finish experiments when I must go to class and for offering encouragement when science is not going my way.

Himanshu Mehra, I want to thank you for all your assistance with experiments. I am thankful that we have become friends during our time working together.

Thank you Xiaozhuo Wang for being both a friend and a mentor. Your quiet, steady presence is a comfort.

Next, I want to express my gratitude to Emily Brown for making me laugh even when I am stressed. I am so happy that we became friends right from the start; your presence surely makes research fun.

I also wish to thank my committee members for agreeing to offer insight and expertise into my project. It is so very generous of you to agree to share your time with me.

Chapter 1. Introduction

Photosynthesis is the process in which the sun's energy is captured and stored as chemical energy, which is used to power life (Blankenship, 2014). Pigment molecules such as chlorophyll allow photosynthetic organisms to absorb light and reaction centers convert that solar energy to chemical energy (Blankenship, 2014). Cyanobacteria, algae, and plants all perform oxygenic photosynthesis, using the photosynthetic electron transport chain. During photosynthesis, NADPH and ATP made by the electron transport chain are used to fix CO_2 in the Calvin-Benson Cycle.

Cyanobacteria are prokaryotic organisms capable of oxygenic photosynthesis. Cyanobacteria are primarily photoautotrophs, meaning that they use light as a source of energy and CO_2 as the sole source of carbon, although some are photoheterotrophs and can use organic compounds as the carbon source. Cyanobacteria are incredibly diverse and can inhabit almost any environment where light is available (Blankenship, 2014).

In photosynthetic eukaryotes including algae and plants, the primary photosynthetic organelle is the chloroplast. Inside of the chloroplast there is the stroma and a highly interconnected internal membrane system known as thylakoids. Thylakoids house the pigment, chlorophyll, as well as an electron transport system. In places, the thylakoids become tightly packed and form grana stacks. Grana stacks are connected to one another by the stroma lamellae. Photosystem II (PSII) is primarily found in the grana, while Photosystem I (PSI) is mostly localized in the stroma lamellae (Blankenship, 2014).

The first complex in the photosynthetic electron transport chain is PSII shown in Figure 1. In PSII, P_{680}, the primary chlorophyll-*a* electron donor, absorbs a photon of visible light. This causes P_{680} to become excited (P_{680}^*) and the electron is transferred to pheophytin-*a*. Next, the electron goes to Q_A, the primary plastoquinone (PQ) electron acceptor. Q_A reduces Q_B, the secondary PQ acceptor. Once Q_B has accepted two electrons and two protons, it forms PQH_2. This plastoquinol molecule can now diffuse out of the reaction center and into the thylakoid membrane. Plastoquinol is replaced by plastoquinone in the reaction center. This series of steps from P_{680}^* to PQH_2 is known as the acceptor side of PSII (Vinyard & Brudvig, 2017). Electrons are then able to be shuttled to PSI by the cytochrome b_6f complex (Blankenship, 2014).

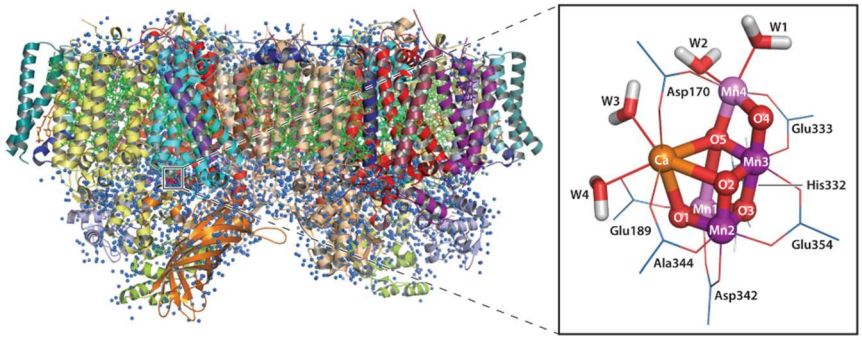

Figure 1: PSII and the oxygen evolving complex (OEC). Taken from (Vinyard & Brudvig, 2017).

On the donor side of PSII, P_{680}^{+} is reduced using electrons from water. PSII contains a tetranuclear Mn cluster, called the oxygen-evolving complex (OEC) which is the site of water oxidation (Blankenship, 2014). As shown in Figure 1, the OEC can be defined as an inorganic cluster of four Mn ions and one Ca ion connected by μ-oxo bridges (Vinyard & Brudvig, 2017). The chemical reaction carried out by the OEC is shown in Eq. 1.

Eq. 1: $$2H_2O \rightarrow O_2 + 4H^+ + 4e^-$$

In the OEC, two water molecules are oxidized to molecular oxygen, producing protons, as well as electrons that can be used by the photosynthetic electron transfer pathway (Blankenship, 2014).

The process of oxidizing water to molecular oxygen requires highly oxidizing reduction potentials (Vinyard, Ananyev, & Charles Dismukes, 2013). In vivo, PSII sustains damage due to reactive oxygen species and must be frequently repaired (Järvi, Suorsa, & Aro, 2015; Komenda, Sobotka, & Nixon, 2012). Rather than replacing the entire complex, only D1, the protein subunit that contains most of the OEC ligating residues and is most likely to be damaged, is replaced (Frankel et al., 2013). The D1 subunit is removed and a new protein is translated and inserted into the PSII complex. Next, the OEC must be photo-assembled for PSII to become functional (Komenda et al., 2012). The net reaction of OEC photo-assembly (Vinyard et al., 2019) is given by Eq. 2:

Eq. 2: $$4Mn^{2+} + Ca^{2+} + 5H_2O \rightarrow (3Mn^{3+})_3Mn^{4+}CaO_5H + 5e^- + 9H^+$$

The process of OEC photo-assembly is a "2-quantum" process. There is a light-dependent step, then a slow light-independent step, and then another light-dependent step, then the OEC is rapidly formed (Radmer & Cheniae, 1971).

Many advances in the study of PSII were made possible by a simple and reproducible protocol to isolate PSII membranes from spinach. Yocum and coworkers developed such a protocol in 1981 (Berthold, Babcock, & Yocum, 1981). This "BBY" method isolates grana stacks from spinach chloroplasts that are highly enriched in PSII and nearly deplete of PSI. BBY stands for Berthold, Babcock, and Yocum, after the scientists who first developed the method.

Higher plant PSII contains the extrinsic subunits PsbO, PsbP, and PsbQ. PsbO is a 33 kDa protein that is found in all oxygenic photosynthetic organisms and has been shown to be a manganese-stabilizing protein (Frankel & Bricker, 1995). PsbO binds to the D1 subunit near the OEC and when PsbO is removed, the OEC is destabilized and O_2 evolution decreases. The extrinsic subunits PsbP and PsbQ, 24 kDa and 17 kDa, respectively, are also present in green algae and plants. When these two extrinsic subunits are removed, oxygen evolution is lowered. However, the evolution can be recovered by adding moderate amounts of calcium (Ghanotakis & Babcock, 1983) and chloride (Andersson et al., 1984). Overall, the extrinsic subunits help to stabilize the oxygen evolving complex and prevent damage, without directly binding to the OEC (Blankenship, 2014). PSII in cyanobacteria contains the extrinsic subunits PsbU and PsbV in addition to PsbO.

In this thesis we sought to explore how PSII is assembled from two aspects. First, we tested multiple methods of chemically removing the OEC to facilitate photo-assembly studies. Next, we characterized the role of the protein PratA in assembly of PSII protein subunits.

Chapter 2. Efficient OEC Depletion in Spinach PSII Membranes

In vitro studies of OEC photo-assembly have been complicated by different biochemical preparations used by different laboratories. We aimed to systematically compare previously published methods to determine the most effective protocol to fully remove PSII extrinsic subunits and the OEC.

In order to study photo-assembly of the OEC, intact PSII membranes must be isolated and depleted of the manganese cluster. Removal of the OEC-stabilizing extrinsic subunits PsbO, PsbP, and PsbQ facilitates the extraction of manganese (Blankenship, 2014). Incubation of BBY membranes with 2 M NaCl removes PsbP and PsbQ (Miyao & Inoue, 1991b). To remove PsbO, PSII membranes can either be incubated with 1 M $CaCl_2$ or a combination of urea and NaCl (Ghanotakis & Yocum, 1990). An alkaline treatment or a reducing agent such as hydroxylamine (NH_2OH) can be used to remove the OEC (Tamura & Cheniae, 1987). Released manganese ions are often chelated by ethylenediamine tetraacetic acid (EDTA).

Miyao and Inoue studied OEC photo-assembly in samples treated with both $CaCl_2$, to remove all extrinsic subunits, and NH_2OH, to remove the OEC. They discovered that PSII membranes that have been treated with NH_2OH can have oxygen evolution restored in the presence of Mn^{2+}, Ca^{2+}, dichlorophenolindophenol (DCIP, an electron acceptor), and Cl^- with illumination (Miyao & Inoue, 1991a).

In other studies by Miyao and Inoue, and in some studies by Cheniae and coworkers, samples were treated with NaCl, to remove only PsbP and PsbQ, and NH_2OH, to remove the OEC. The groups showed that when compared, to control PSII membranes, approximately 66% of the O_2 activity was restored in the presence of Mn^{2+} and Ca^{2+} (Chen, Kazimir, & Cheniae, 1995; Miyao & Inoue, 1991b).

Brudvig and Miller studied OEC photo-assembly in BBY membranes treated only with NH_2OH. The group showed that their treated samples recovered O_2 evolution activity when Mn^{2+} and Ca^{2+} were added back (Miller & Brudvig, 1989).

Dismukes and coworkers introduced an alkaline shock treatment that does not require the use of high salt concentrations or NH_2OH. The group's observations were that 70% of the O_2 activity of the treated samples was restored in the presence of Ca^{2+} and Mn^{2+}. They also showed that 0.1 – 0.5 M Ca^{2+} and 100 – 250 μM Mn^{2+} is required to produce the maximum photo-assembly yield (Baranov et al., 2004).

Given the wide range of reported methods, this chapter describes a side-by-side comparison of these approaches in terms of extrinsic subunit composition, manganese content, O_2 evolution activity, and photo-assembly yield.

2.1 Methods:

BBY Protocol:

Spinach PSII membrane samples (BBYs) were prepared according to Berthold et al. (1981) with 2-(N-morpholino)ethanesulfonic acid (MES) used in later steps instead of 4-(2-hydroxyethyl)-1- piperazineethanesulfonic acid (HEPES) (Ghanotakis & Babcock, 1983). Ethylene glycol was used as a cryoprotectant to store samples at -80° (Beck, de Paula, & Brudvig, 1986).

Methods for removing the OEC:

To prepare all samples, approximately 40 mg of chlorophyll (Chl) as BBYs were first thawed and washed twice with 50 mM MES pH 6.0, 10 mM $CaCl_2$, 15 mM NaCl, 400 mM sucrose, and 0.01% (v/v) Triton X-100 (minimal wash buffer). The entire process was done on ice with only dim green LED light. All centrifugation steps occurred for 20 minutes at 38,000 x g and 4°C. Following centrifugation, all pellet resuspensions were done using a brush and homogenized manually using a tissue grinder. Chl concentration was measured and 2 mg of Chl was saved as "Control BBYs," using sucrose as a cryoprotectant for storage at -80°C. Following this, the remaining sample was divided evenly, and each was given a different treatment.

Protocol I – $CaCl_2$ and NH_2OH. One-fourth of the above sample was resuspended to 0.5 mg Chl mL^{-1} in 50 mM MES pH 6.0, 1 M $CaCl_2$, and 400 mM sucrose ($CaCl_2$ treatment) and incubated on ice for 1 hour, homogenizing periodically. This high $CaCl_2$ wash was done to remove all extrinsic subunits. The sample was then centrifuged, resuspended again to 0.5 mg Chl mL^{-1} in high $CaCl_2$ buffer and immediately spun down. In order to remove excess $CaCl_2$, the sample was washed in high chloride buffer containing 50 mM MES pH 6.0, 25 mM $CaCl_2$, 200 mM NaCl, 400 mM sucrose, and 0.01% (v/v) Triton X-100. This step was repeated a second time. Next, in order to remove the OEC, the sample was resuspended in 50 mM MES pH 6.0, 10 mM $CaCl_2$, 15 mM NaCl, 400 mM sucrose, 5 mM EDTA, 0.01% (v/v) Triton X-100, and 5 mM NH_2OH (NH_2OH and EDTA treatment) to a final concentration of 0.5 mg Chl mL^{-1}. The sample was incubated on ice for 10 minutes, homogenizing periodically, and then spun down. The PSII membranes were then resuspended in EDTA wash buffer, composed of 5 mM MES pH 6.0, 10 mM $CaCl_2$, 15 mM NaCl, 400 mM sucrose, 1 mM EDTA, and 0.01% (v/v) Triton X-100. The sample was spun down and resuspended in EDTA wash buffer twice more. The sample was again centrifuged and then resuspended in minimal wash buffer twice. The sample was then spun down and resuspended in a minimal amount of storage buffer containing 25 mM MES and 400 mM sucrose. Aliquots were stored at -80°C.

Protocol II – NaCl and NH_2OH. A parallel sample was resuspended in 50 mM MES pH 6.0, 25 mM $CaCl_2$, 2 M NaCl, and 400 mM sucrose (NaCl treatment buffer) to a final concentration of 0.5 mg Chl mL^{-1}. The sample was incubated on ice for 1 hour, homogenizing periodically, spun down, and resuspended to 0.5 mg Chl mL^{-1} in the same buffer. It was immediately centrifuged this time and then washed twice in high chloride wash buffer. After centrifuging again, the sample was resuspended in NH_2OH and EDTA treatment buffer to 0.5 mg Chl mL^{-1}. The sample was incubated on ice for 10 minutes, homogenizing periodically, then

spun down and resuspended in EDTA wash buffer. The sample twice more underwent centrifugation and resuspension in EDTA wash buffer. Next, the sample was washed twice with minimal wash buffer. The sample was then washed twice with minimal storage buffer. The final sample was aliquoted and stored at -80°C.

Protocol III – NH_2OH. Another parallel sample was resuspended in NH_2OH and EDTA treatment buffer to 0.5 mg Chl mL^{-1} final concentration. The sample was incubated on ice for 10 minutes, periodically homogenized, and then spun down. Following centrifugation, the sample was resuspended in EDTA wash buffer. The sample was then centrifuged and washed twice more with EDTA wash buffer. Next the sample was washed twice with minimal wash buffer. Lastly, this sample was washed twice with minimal storage buffer and the final sample was aliquoted and stored at -80°C.

Protocol IV – Alkaline Shock. The final sample was treated with N-Cyclohexyl-2-aminoethanesulfonic acid (CHES). Following the initial wash steps, the sample was resuspended in a minimal volume of 5 mM MES pH 6.0, 10 mM $CaCl_2$, 15 mM NaCl, 400 mM sucrose (low MES buffer), using only a brush. Next, buffer containing 20 mM CHES pH 9.4, 10 mM $CaCl_2$, 15 mM NaCl, 400 mM sucrose, 1 mM EDTA, and 200 mM $MgCl_2$ (CHES buffer) was added until the final concentration was 0.25 mg Chl mL^{-1}. The sample was quickly homogenized and then EDTA wash buffer was added. The time between adding the CHES buffer and the EDTA wash was between 40 and 90 seconds. The sample was centrifuged and washed in EDTA wash buffer three more times. Then the sample was then washed twice in minimal wash buffer. Finally, the sample was washed twice in minimal storage buffer and the final sample was aliquoted and stored at -80°C.

Each of these protocols was done as biological replicates. For each replicate, the protocols were performed in parallel on the same day.

Chl Concentrations:

Chl concentration was measured by acetone extraction with extinction coefficients from Porra et al. (Porra, R. J., Thompson, W. A., Kriedemann, 1989). Using a calibrated capillary, 5 µL of sample was added to 5 mL of 80% (v/v) acetone/water. 1 mL of the suspension was transferred to a microcentrifuge tube and spun down at ~10,000 rpm for 1 minute. Following centrifugation, the supernatant was immediately decanted, and the absorbance was measured at 647 nm and 664 nm. Concentration of total chlorophyll was calculated according to the following formula.

$$[\text{Chl-a + b}]\left(\frac{\text{mg}}{\text{mL}}\right) = 17.76 * \text{A}_{647} + 7.34 * \text{A}_{664}$$

This formula calculates the total chlorophyll in the sample, including Chl-*a* and Chl-*b*. A_{647} is the absorbance measured at 647 nm. A_{664} is the absorbance measured at 664 nm.

O_2 Evolution:

Activity of all of the samples was measured as the rate of O_2 evolution. The O_2 evolution rate was measured using a Hansatech Oxygraph system. Illumination to induce O_2 evolution was

provided by a red LED (λ_{max} = 623 nm, ~4 W optical power). All O_2 assays were performed at 25°C in 25 mM MES, pH 6.0, 25 mM $CaCl_2$, 50 mM NaCl, 1 mM potassium ferricyanide, 0.25 mM phenyl-1,4-benzoquinone (PPBQ) (recrystallized two times from ethanol), and 5-10 μg chlorophyll of prepared samples.

Total Mn:

In order to quantify Mn content, Electron Paramagnetic Resonance (EPR) spectroscopy was performed. To prepare samples for EPR, 0.15 mg of chlorophyll as treated PSII membranes was digested in 14 M HNO_3. Samples were incubated at room temperature before being centrifuged to remove residual debris. Samples were transferred to quartz EPR tubes and the spectra were measured on a Bruker EMX spectrometer equipped with a standard cavity and an ESR900 helium flow cryostat. Experimental parameters were microwave frequency, 9.47 GHz; microwave power, 4 mW; modulation frequency, 100 kHz; modulation amplitude, 20 G; sweep time, 42 s; conversion time, 21 ms; time constant, 82 ms; and temperature 8.4±0.2 K.

Photo-assembly:

Thawed and homogenized samples were added to photo-assembly buffer and freshly prepared DCIP. Samples prepared according to methods I, II, and III were tested. All photo-assembly reactions contained 0.25 mg mL^{-1} chlorophyll, 25 mM MES pH 6.0, 400 mM sucrose, 8 mM $NaHCO_3$, 40 mM $CaCl_2$, 0.16 mM $MnCl_2$ and 10 μM DCIP. NaCl was added to make the final Cl^- concentration either 100 mM or 750 mM.

Photo-assembly was induced by placing the reactions in an incubator at 25°C under 50 μE m^{-2} s^{-1} illumination with gentle rocking. After 20 minutes, the rate of O_2 evolution was recorded as described above.

SDS-PAGE:

SDS-PAGE was performed using 12% polyacrylamide gels. All samples had 3 μg of chlorophyll denatured on ice using 2% lithium dodecyl sulfate and 2% β-mercaptoethanol. Proteins were visualized by silver staining.

Western Blots:

Western blots of samples were performed immediately following SDS-PAGE. Gels were blotted onto PVDF membrane and then blocked for 1 hour at room temperature in non-fat milk. The primary antibodies used were α-PsbO, a gift from Dr. Bricker, α-PsbP from Agrisera, and α-PsbQ from Agrisera. The dilutions for the primary antibodies are as follows: α-PsbO 1:10,000, α-PsbP 1:1000, α-PsbQ 1:10,000. The secondary antibody was a HRP-conjugated goat anti-rabbit secondary antibody from Invitrogen at a dilution of 1:10,000. Chemiluminescence (ECL Clarity, Bio-Rad) was used for detection.

2.2 Results:

O_2 Evolution of control BBYs:

Table 1 shows the oxygen evolution rate of the control BBYs for the different biological replicates. These BBYs were prepared on different days and O_2 evolution was measured after washing stored BBYs twice with minimal wash buffer. For each O_2 evolution reaction, 5 µg of chlorophyll were used.

	Replicate 1	Replicate 2	Replicate 3
O_2 evolution rate	592	444	331
Standard Error	1	1	1

Table 1: Oxygen evolution rates of control BBYs. Rates are given in µmol O_2 (mg Chl)$^{-1}$ h^{-1}.

O_2 Evolution of 4 treatments:

Table 2 gives the data for the oxygen evolution rates of PSII membranes with different treatments. For each replicate, all oxygen evolution measurements were performed on the same day. The oxygen evolution rates for depleted OEC PSII membranes are relatively low for treatments with $CaCl_2$ and NH_2OH, and NaCl and NH_2OH. The oxygen evolution rate increases noticeably, however, for treatment with NH_2OH. Samples treated with CHES have very high oxygen evolution rates.

	Replicate 1	Replicate 2	Replicate 3
Protocol I	7.51 (1.27%)	4.06 (0.915%)	0.462 (0.139%)
Standard Error	0.18	0.07	0.008
Protocol II	4.96 (0.838%)	2.06 (0.463%)	4.64 (1.40%)
Standard Error	0.0158	0.00167	0.0710
Protocol III	19.5 (3.29%)	24.3 (5.48%)	21.9 (6.59%)
Standard Error	0.0	0.1	0.1
Protocol IV	319 (54.0%)	217 (48.9%)	309 (93.5%)
Standard Error	1.3	0.8	0.3

Table 2: Oxygen evolution rates of treated PSII membranes. Rates are given in µmol O_2 (mg Chl)$^{-1}$ h^{-1}. The percentage of the control O_2 evolution rate is shown in parentheses.

Mn content of 4 treatments:

The different methods for preparing apo-OEC PSII membranes were analyzed using EPR. The relative Mn abundance was measured for each replicate and averaged. Data were normalized to control PSII membranes (no treatment). The average relative Mn abundance for Protocol I, $CaCl_2$ and NH_2OH treatment, was 0.032 with a standard error of 0.032. For treatment with NaCl and NH_2OH, Protocol II, no Mn was detected. Protocol III, treatment with NH_2OH, had 0.064 as the average relative Mn abundance and a standard error of 0.0071. Finally, the

average relative Mn abundance of samples treated with CHES, Protocol IV, was 0.410 with a standard error of 0.062.

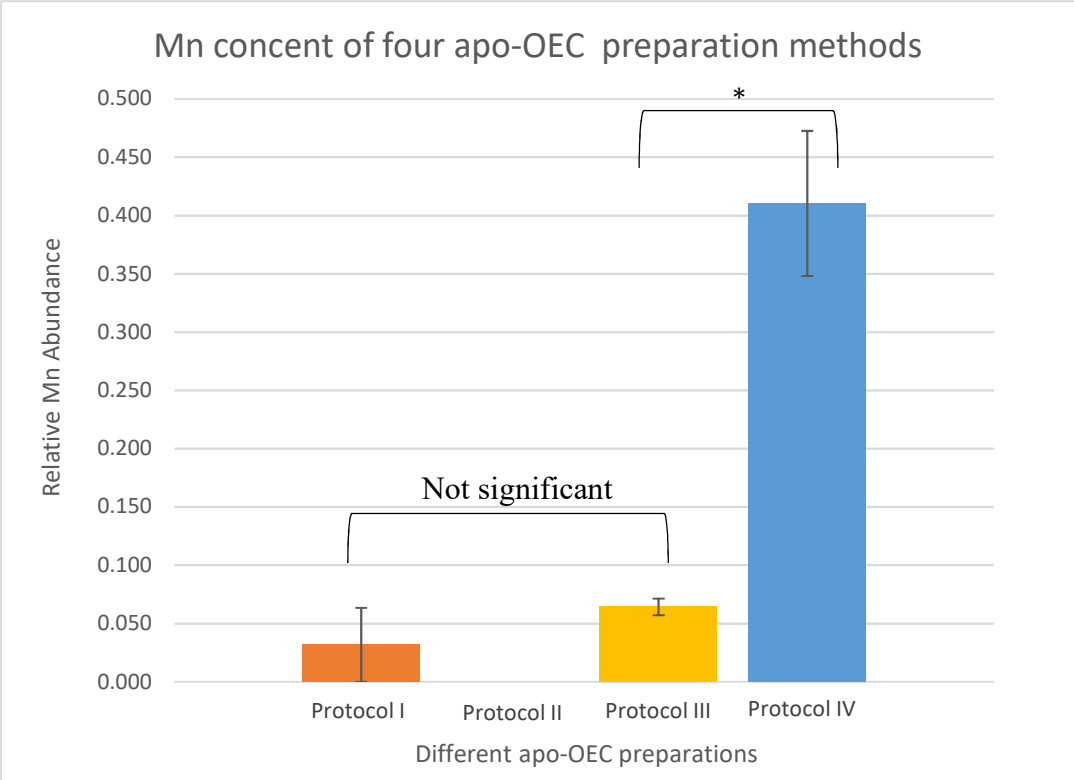

Figure 2: The relative Mn abundance contained in the different preparations of PSII membranes. Indication of statistical significance between replicates is denoted by (*).

Photo-assembly yields:

Photo-assembly yields were measured for each of the OEC depletion methods, except for method IV, because relative Mn content and O_2 evolution rates were very high. These data show the yield of photo-assembly after 20 minutes of light exposure. Each of the measurements was done in triplicate and the averages of these data were used to generate graphs.

For both high (750 mM) and low (100 mM) chloride, the data show that photo-assembly yield is lowest for samples prepared with $CaCl_2$ and NH_2OH and highest for samples prepared with only NH_2OH. Photo-assembly samples containing higher chloride concentrations also show a higher yield than those with low chloride.

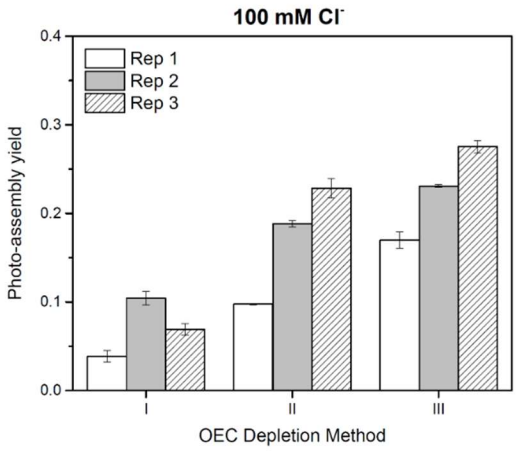

Figure 3: Photo-assembly yields of the different preparation methods of apo-OEC PSII under 100 mM Cl^- conditions.

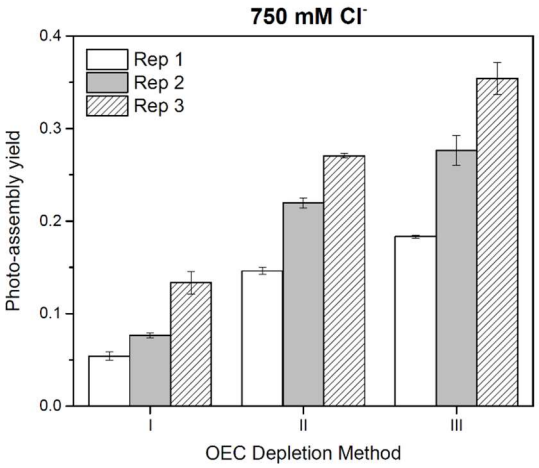

Figure 4: Photo-assembly yields of the different preparation methods of apo-OEC PSII under 750 mM Cl^- conditions.

Silver Staining and Western Blots:

The different methods of preparing depleted OEC PSII, were analyzed with SDS-PAGE and immunoblotting.

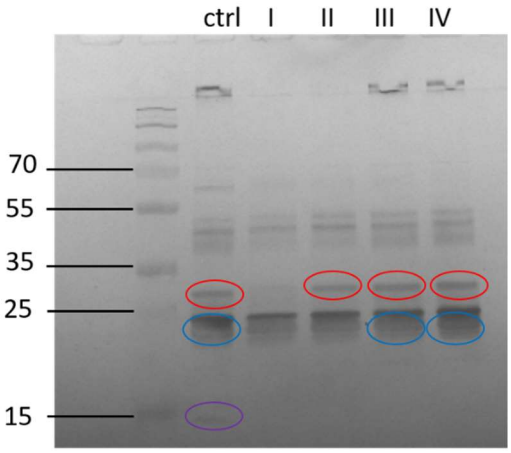

Figure 5: Replicate 1 silver stain after SDS-PAGE. Lane 2-control BBYs. Lane 3 shows Protocol I sample. Lane 4 shows Protocol II sample. Lane 5 shows Protocol III sample. Lane 6 shows Protocol IV sample. The presence of PsbO is shown as red ovals, the presence of PsbP is shown as blue ovals, and the presence of PsbQ is shown as a purple oval.

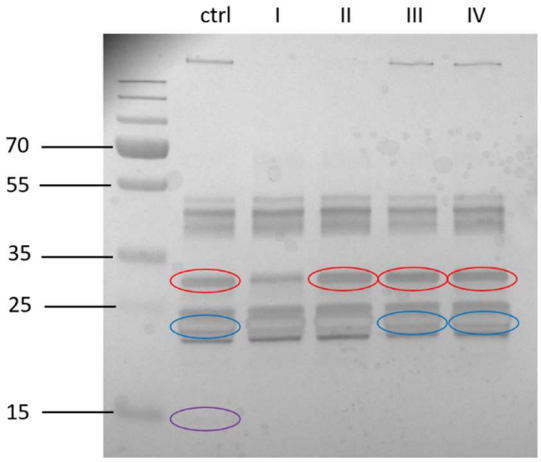

Figure 6: Replicate 2 silver stain after SDS-PAGE. Lane 2 shows control BBYs. Lane 3 shows Protocol I sample. Lane 4 shows Protocol II sample. Lane 5 shows Protocol III sample. Lane 6 shows Protocol IV sample. The prence of PsbO is shown as red ovals, the presence of PsbP is shown as blue ovals, and the presence of PsbQ is shown as purple ovals.

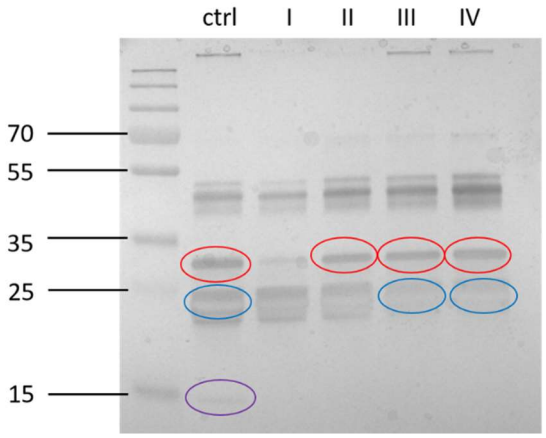

Figure 7: Replicate 3 silver stain. Lane 2 shows control BBYs after SDS-PAGE. Lane 3 shows Protocol I sample. Lane 4 shows Protocol II sample. Lane 5 shows Protocol III sample. Lane 6 shows Protocol IV sample. The presence of PsbO is shown as red ovals, the presence of PsbP is shown as blue ovals, and the presence of PsbQ is shown as purple ovals.

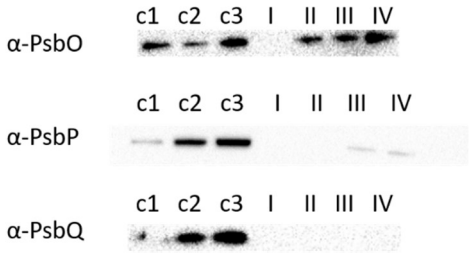

Figure 8: Western blot analysis of Replicate 1 samples. c1- 25% control BBY, c2- 50% control BBY, c3- 100% control BBY. All of the protocol samples as well as c3 have 1 µg Chl loaded.

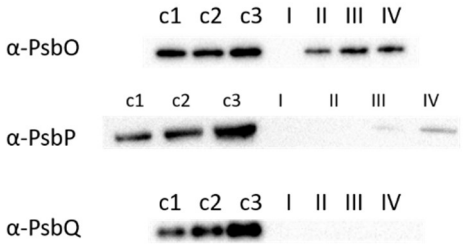

Figure 9: Western blot analysis of Replicate 2 samples. c1- 25% control BBY, c2- 50% control BBY, c3- 100% control BBY. All of the protocol samples as well as c3 have 1 µg Chl loaded.

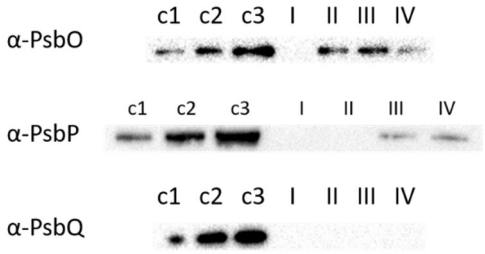

Figure 10: Western blot analysis of Replicate 3 samples. c1- 25% control BBY, c2- 50% control BBY, c3- 100% control BBY. All of the protocol samples as well as c3 have 1 µg Chl loaded

2.3 Discussion:

Protocol I Samples:

For replicate 1, the rate of oxygen evolution for the control BBYs was 592 µmol O_2 (mg Chl)$^{-1}$ h^{-1}. After treatment with $CaCl_2$ and NH_2OH, the rate of oxygen evolution fell dramatically to 7.51 µmol O_2 (mg Chl)$^{-1}$ h^{-1}, 1.27% of the original oxygen evolution. According to the Western blot data, none of the extrinsic subunits were present in the samples and EPR analysis revealed that the relative Mn abundance was 0.095 with an error of 0.032.

For replicate 2, the oxygen evolution rate of the control was 444 µmol O_2 (mg Chl)$^{-1}$ h^{-1}. Following $CaCl_2$, NH_2OH treatment, the rate of oxygen evolution fell to 4.06 µmol O_2 (mg Chl)$^{-1}$ h^{-1}. This marks a 99% decrease in the rate of oxygen evolution. Again, all of extrinsic subunits were removed by this treatment and EPR showed no presence of Mn.

The control oxygen evolution rate of replicate 3 was 331 µmol O_2 (mg Chl)$^{-1}$ h^{-1} which dropped by 99.9% to 0.462 µmol O_2 (mg Chl)$^{-1}$ h^{-1} following $CaCl_2$, NH_2OH treatment. All extrinsic subunits were removed through the washes and EPR revealed that no Mn was present.

All replicates of samples treated with $CaCl_2$ and NH_2OH showed the lowest photo-assembly yield of the three preparation methods. This data is true for both 100 mM Cl^- and 750 mM Cl^- conditions. When comparing Cl^- concentration conditions, however, the high Cl^- condition resulted in higher photo-assembly. It should also be noted that each replicate demonstrates greater photo-assembly yields. This indicates that technique was improved each time a sample preparation was performed.

Protocol II Samples:

For replicate 1 with treatment with NaCl and NH_2OH, the oxygen evolution rate decreased from 592 μmol O_2 (mg Chl)$^{-1}$ h^{-1} to 4.96 μmol O_2 (mg Chl)$^{-1}$ h^{-1}, 0.838% of the control. Immunoblot analysis revealed that PsbO was present, but PsbP and PsbQ had been removed. EPR analysis showed that no Mn was present.

For replicate 2, the oxygen evolution rate decreased to 0.436% of the control. The control oxygen was 444 μmol O_2 (mg Chl)$^{-1}$ h^{-1} and after treatment, went to 4.06 μmol O_2 (mg Chl)$^{-1}$ h^{-1}. Western blot analysis revealed that PsbO was present, but PsbP and PsbQ had been removed. No Mn was present, based on EPR analysis.

The control oxygen evolution of replicate three was measured to be 331 μmol O_2 (mg Chl)$^{-1}$ h^{-1}. Following treatment with NaCl and NH_2OH, the oxygen evolution rate of replicate three decreased to 4.64 μmol O_2 (mg Chl)$^{-1}$ h^{-1}, 1.40% of the control. Analysis of the Western blot revealed that PsbO was present, but PsbP and PsbQ had been removed. EPR showed that no Mn was present.

The photo-assembly data of samples treated with NaCl and NH_2OH show that these samples have higher photo-assembly yields than samples prepared according to method I, but lower yields than those prepared by method III. These data are true under both 100 mM Cl^- and 750 mM Cl^- conditions. However, when the high chloride condition is compared to the low chloride conditions, samples under high chloride conditions exhibit greater photo-assembly yields. Furthermore, each replicate demonstrates greater photo-assembly yields. This indicates that technique was improved each time a sample preparation was performed.

Protocol III Samples:

Replicate 1 of NH_2OH treatment showed a 96.7% drop in oxygen evolution from the control (592 μmol O_2 (mg Chl)$^{-1}$ h^{-1} to 19.5 μmol O_2 (mg Chl)$^{-1}$ h^{-1}). Western blots show that all of PsbQ was removed, as was most of PsbP, but PsbO was still present.

A 94.5% decrease in oxygen evolution was observed, following treatment of the replicate 2 sample with NH_2OH. As with the replicate 1 samples, PsbO was present, PsbQ was absent, and most of PsbP had been washed away with this method.

After treatment with NH_2OH, the oxygen evolution rate decreased from 331 μmol O_2 (mg Chl)$^{-1}$ h^{-1} to 21.9 μmol O_2 (mg Chl)$^{-1}$ h^{-1}. This marks a 93.4% drop in oxygen evolution. Analysis of the samples using a Western blot showed that PsbO was present, PsbP was depleted, and PsbQ was absent.

The average relative Mn abundance of method III samples as analyzed with EPR was 0.064 with a standard error of 0.007. Samples treated with NH_2OH produced the highest photo-assembly yields out of protocols I, II, and III. This is true under both high and low chloride conditions. Notably, under 750 mM Cl^- conditions, photo-assembly is higher than samples under 100 mM Cl^- conditions. The data also demonstrate that for each replicate, the photo-assembly yield increases. This implies that technique was improved with each sample preparation.

Protocol IV Samples:

CHES-treated PSII membranes in replicate 1 showed oxygen evolution rates fall by 46.0% compared to the control. Western blots showed that PsbQ was removed, a lot of PsbP was removed, and PsbO was still present in the sample.

The second replicate of CHES-treated PSII membranes showed that the oxygen evolution decreased by 51.1% from the control. PsbO was present, as was a depleted amount of PsbP, and no PsbQ was present in the sample, as shown on a Western blot.

Replicate 3 of the CHES-treated BBYs showed that oxygen evolution dropped by 6.52%, from 331 μmol O_2 (mg Chl)$^{-1}$ h^{-1} to 309 μmol O_2 (mg Chl)$^{-1}$ h^{-1}. PsbP was present in a depleted amount, PsbO was present, and no PsbQ was in the sample.

Samples prepared according to method IV, had an average relative Mn abundance of 0.41 with a standard error of 0.06. Because the Mn abundance was so high, photo-assembly assays were not performed.

Overview of the Different Protocols:

Statistical analysis revealed that there is no significant difference between Mn abundance using Protocols I, II, and III. However, the Mn abundance using Protocol IV, the alkaline shock treatment, is significantly higher ($p = 0.001$).

Protocol I consistently removed all the extrinsic subunits, PsbO, PsbP, and PsbQ. Protocol II removed PsbP and PsbQ but not PsbO. Protocol III removed PsbQ, a lot of PsbP, but not PsbO, and Protocol IV similarly removed PsbQ, a lot of PsbP, but not PsbO.

When comparing each protocol's oxygen evolution rates to the control, Protocols I, II, and III had rates that were significantly different from the control. For Protocol I and Protocol II, statistical analysis revealed that the two oxygen evolution rates were not significantly different from one another. However, Protocols III and IV were significantly different from one another and from the other two protocols (Protocol III vs. Protocol I, $p=0.002$; Protocol IV vs. Protocol III, $p=0.001$; Protocol IV vs. Protocol I, $p = 0.0011$). When compared to the control, the oxygen evolution rate of Protocol IV was determined not to be statistically significant.

For the first three preparations (I, II, and III), photo-assembly yields were highest under high Cl^- conditions (750 mM).

Reproducibility:

Data between replicates was difficult to reproduce. With each replicate preparation, it seems that technique improved and thus influenced the results. In general, it appears that all samples in the first replicate have higher Mn abundance, photo-assembly yields, and extrinsic subunit compositions. This can be attributed to unfamiliarity with the preparation protocols. With experience of the protocol, the data for replicates 2 and 3 are more similar to one another. Western blot loading controls, similarly were difficult to reproduce, which affects result analysis. With silver staining, it is difficult to resolve PsbP, but the extrinsic protein appears clearly in

blots. Furthermore, in silver staining, there appears to be residual PsbO, but that is not observed in the Western blots.

Chapter 3. Role of PratA in PSII Assembly

Working with the cyanobacterium *Synechocystis* sp. PCC 6803, Nickelsen and coworkers identified a 36 kDa protein that they termed PratA for "processing associated TPR protein," (Klinkert et al., 2004). TPR stands for tetratricopeptide repeat (Bohne, 2016). PratA can either be attached to the membrane due to its interaction with the D1 subunit of PSII, or it can occur in the periplasm as a soluble ~200 kD complex (Klinkert et al., 2004). TPR proteins generally contain a degenerate protein-protein interaction motif consisting of multiple repeats of 34 amino acids making two antiparallel, amphipathic α-helices. TPRs also play an important role in the biogenesis of the thylakoid membrane (Bohne, 2016). These proteins typically have nonglobular folds, which give them an elongated solenoid-like structure that serves as a scaffold for the binding of protein ligands (Bohne, 2016).

In studying PratA, Klinkert et al. made a *pratA* mutant that lacks PratA, by inserting a kanamycin resistance cassette within the reading frame. Although the chlorophyll content remained relatively constant, the photoautotrophic growth rate of the mutant was significantly reduced compared to that of the wild type. Next, using pulse-labeling experiments, they showed that in the *pratA* mutant, there was an absence of mature D1, leading to the conclusion that PratA is involved in the C-terminal processing of D1 protein. To test whether PratA interacts with D1 or CtpA, the protease that cleaves the C-terminus of D1, the group performed yeast two-hybrid experiments. They were unable to determine if PratA interacts with CtpA, because CtpA in yeast impaired the import of fusion proteins into the nucleus. However, the group was able to show using yeast two-hybrid assays that PratA does interact with the C terminus of pD1 (Klinkert et al., 2004).

In follow up paper, Nickelsen and coworkers made more notable observations about PratA. Performing pull-down experiments of mature D1 and precursor D1 when incubated with periplasmic proteins from both wild-type and *pratA* mutant cells, they showed that native PratA was pulled down from both mD1 and pD1 in the wild type, and not at all in the *pratA* mutant (Stengel et al., 2012). While isolating and concentrating the periplasm samples, the group noticed a difference in color between the wild type and *pratA* mutant. They used atomic absorption spectrometry to measure the concentrations of Mn and Fe present in the periplasm samples and noted that the amount of Mn in the *pratA* mutant was significantly lower than that of the wild type (Stengel et al., 2012). Next, they tested whether PratA itself could bind Mn using circular dichroism (CD) measurements and electron paramagnetic resonance (EPR). Using CD, they noticed that when PratA was incubated with Mn^{2+} present, a conformational change was observed when compared to the PratA without Mn^{2+} present (Stengel et al., 2012). Samples of Mn^{2+}-containing PratA showed a smaller EPR amplitude, indicating that PratA was binding and thus lowering the free Mn^{2+} present. Then, when denatured PratA was present, the free Mn^{2+} concentration increased again, demonstrating that PratA binding to Mn^{2+} requires a specific conformation (Stengel et al., 2012). The group also performed competition experiments and determined that PratA specifically binds Mn^{2+}, even with 10-fold excess of Ca^{2+} or Mg^{2+} (Stengel et al., 2012).

PratA has been shown to be primarily localized to the periplasm in regions connecting the plasma membrane (PM) and thylakoid membrane (TM). These regions where PratA is localized are termed PratA defined membranes (PDM) (Klinkert et al., 2004). To study this further, Stengel et al. used immunogold labeling experiments using an α-PratA antibody. The group determined that the PratA was localized to distinct clusters which they termed "biogenesis centers." The group found that pD1 also localized in clusters but were unable to determine colocalization of PratA and pD1 in the same sample. However, the group reports that ultrastructural analysis supports the conclusion that both PratA and pD1 are colocalized in these structures. When PratA is absent, the organization of the structures is lost (Stengel et al., 2012).

We aimed to measure photo-assembly in vitro as described in Chapter 2 in the presence and absence of purified PratA. If PratA is indeed acting as an assembly factor involved in delivering Mn^{2+} to apo-OEC-PSII, we hypothesized that PratA would change photo-assembly yields and potentially affect the rate of photo-assembly.

3.1 Methods:

Expression of PratA in *E. coli*:

The *pratA* gene from the cyanobacterium *Synechocystis* sp. PCC 6803 was codon optimized for *Escherichia coli* and synthesized by VectorBuilder. Initial attempts of heterologous expression were unsuccessful; PratA was found in inclusion bodies. To improve solubility, PratA was expressed as a His-tagged, TEV protease-cleavable fusion protein using the Expresso Solubility and Expression Screening System purchased from Lucigen. Overhangs were added to the *pratA* gene using PCR. *E. coli* cultures were transformed with *pratA* and pSOL vectors containing seven different fusion systems.

Expression of the PratA fusion protein is controlled under the $rhaP_{BAD}$ promoter as defined by Lucigen (Expresso, 2015). *E. coli* was grown to 0.4 OD_{600} then induced with 0.2% (w/v) L-rhamnose for four hours. Cells were pelleted, washed, and lysed with BugBuster. Following centrifugation, crude soluble protein was flowed through a gravity Ni^{2+}-NTA column. The column was thoroughly washed with Wash Buffer containing 50 mM NaH_2PO_4, 300 mM NaCl, 15 mM imidazole, with a final pH of 8.0. Protein was then eluted in Elution Buffer containing 50 mM NaH_2PO_4, 300 mM NaCl, 500 mM imidazole with a pH of 8.0. Fractions containing protein were pooled and incubated overnight with 5 mM DTT and TEV protease at 4°C. The TEV protease was purified in our laboratory, using the pDZ2087 plasmid in *E. coli* (Raran-Kurussi S., 2017). Protein sample containing PratA was then passed through a desalting column to remove imidazole and DTT. Finally, the protein was put through a second Ni^{2+}-NTA column and flow through was collected. Fractions containing PratA were pooled, concentrated, and subjected to size-exclusion chromatography. The purified protein was frozen in 25% (v/v) glycerol and stored at -80°C.

Binding Experiments:

Apo-OEC PSII was prepared according to the method I protocol discussed in Chapter 2.

Approximately 10 equivalents of PratA were incubated with 1 equivalent of either untreated PSII membranes or apo-OEC-PSII membranes for 45 minutes at 4°C. Samples were centrifuged, decanted, and re-suspended and homogenized in fresh buffer five times to remove unbound protein.

Pull Downs and Mass Spectrometry:

His_6-Bla-PratA was loaded onto a Ni^{2+}-NTA column. Thylakoid membranes, isolated from wild type *Synechocystis* sp. PCC 6803, and solubilized with 1% n-dodecyl β-D-maltoside were run over the column. The column was washed extensively with Wash Buffer and then eluted with Elution Buffer. A control experiment was performed in parallel in which the His_6-Bla-PratA was not loaded onto the column. Total eluted protein was analyzed by LC-MS/MS on an Orbitrap spectrometer by the company Bioproximity.

Antibody Production:

Purified PratA was sent to PhytoAB to produce an α-PratA polyclonal primary antibody in rabbit.

Crystallography Trials:

Purified PratA was sent to the High Throughput Crystallization Screening Center at the Hauptman-Woodward Medical Research Institute in Buffalo, New Yok for preliminary crystallography trials. Later trials at LSU optimized protein concentration using the Pre-Crystallization Test kit from Hampton Research. Hanging drop vapor diffusion was performed using a variety of commercial kits available in the Newcomer and Vinyard laboratories.

3.2 Results:

Plasmid map of the PratA construct:

The final PratA plasmid was isolated using the Viogene Mini Plus Plasmid DNA extraction system. The plasmid construct was verified with DNA sequencing. The primers used for sequencing were a pRham forward primer and a T7 terminator reverse primer.

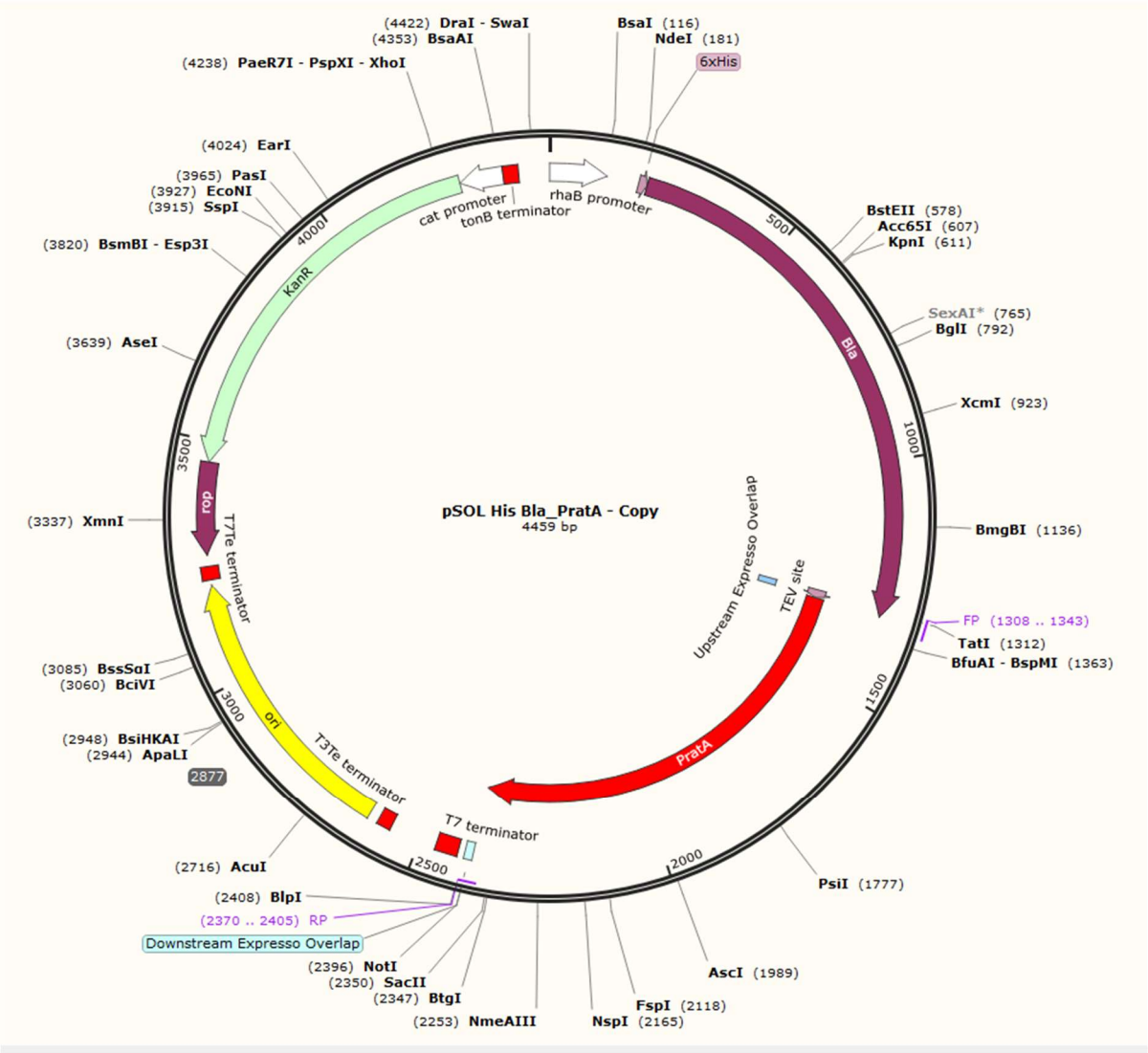

Figure 11: Plasmid map of the PratA construct.

Expression of PratA in *E. coli*:

The fusion partners tested in the Lucigen Expresso kit were AFV (hypothetical protein from Acidianus filamentous virus-1), SlyD (FKBP-type peptidyl-prolyl cis-trans isomerase), Tsf (elongation factor Ts), SUMO (Small Ubiquitin-like Modifier), Bla (β-lactamase), and MBP (maltose-binding protein). Figure 12 shows soluble proteins produced by fusion partners. Of these fusion partners, Tsf and Bla produced soluble protein.

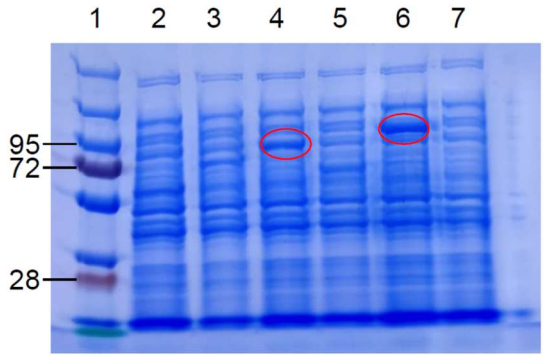

Figure 12: SDS-PAGE analysis of fusion partners was stained with Coomassie. Lane 1- ladder, Lane 2- AFV, Lane 3- SlyD, Lane 4- Tsf, Lane 5- SUMO, Lane 6- Bla, Lane 7- control. Red ovals indicate successful protein expression.

PratA Purification:

Figure 13 shows the process of purifying PratA. The predicted molecular mass of the His_6-Bla-PratA fusion protein is 79.9 kDa. The fusion protein was induced using 0.2% rhamnose (lane 2) then purified by Ni^{2+}-NTA affinity chromatography (lane 3). Following cleavage of the fusion protein by TEV (lane 4), the expected molecular weight of PratA is 38.6 kDa. Purified PratA (lane 5) is isolated as flow through from a second Ni^{2+}-NTA column.

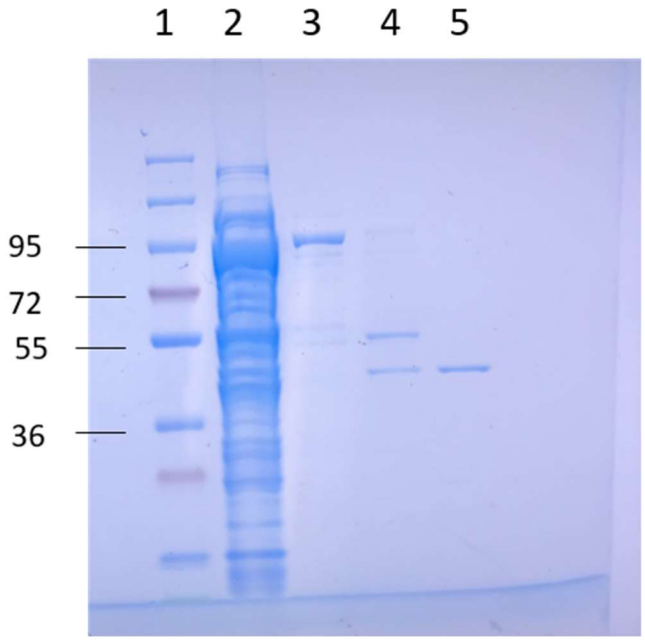

Figure 13: Lane 2- total soluble protein after induction, Lane 3- Purified His_6-Bla-PratA, Lane 4- His_6-Bla-PratA following treatment with TEV, Lane 5- Purified PratA

Binding Experiments:

SDS-PAGE analysis was performed on samples from binding experiments. All samples for SDS-PAGE contained 3 µg of chlorophyll. Samples were denatured on ice using 2% LiDS and 2% β-mercaptoethanol. Proteins were visualized by Coomassie staining. The gel shows no difference between control incubated with PratA and those without PratA. It also shows no difference between apo-OEC-PSII membranes incubated with PratA and those without PratA.

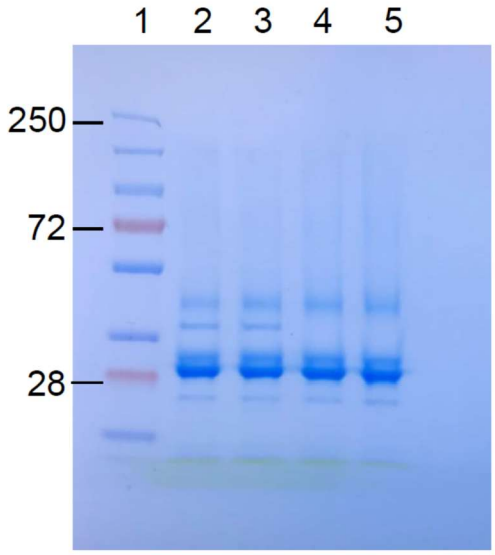

Figure 14: SDS-PAGE analysis of binding experiment samples and stained with Coomassie. Lane 2- control PSII membranes, Lane 3- Control PSII membranes incubated with PratA and washed, Lane 4- apo-OEC-PSII membranes, Lane 5- apo-OEC-PSII membranes incubated with PratA and washed.

Western blot analysis was performed on samples from binding experiments using an α-PratA antibody at a dilution of 1:5000 and a goat anti-rabbit secondary antibody at a dilution of 1:10,000.

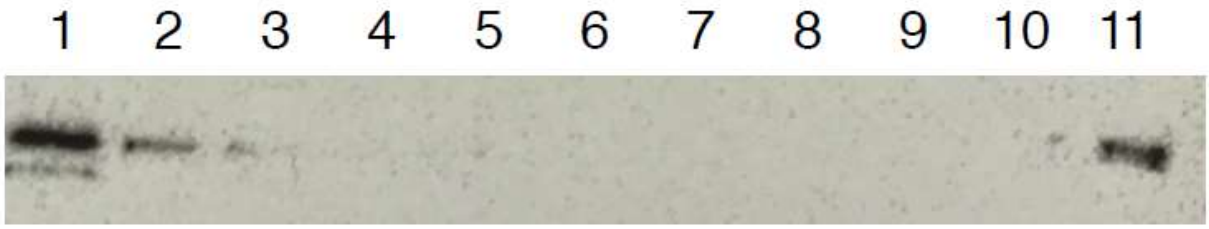

Figure 15: Immunoblot of binding assay products. Lanes 1-3 show positive PratA controls, ranging from 1.44 µg – 0.36 µg PratA. Lanes 4-11: $CaCl_2$ washed PSII membranes incubated with 0.047 µg– 1.44 µg PratA.

Pull Down Experiments:

Three biological replicates of pull-down experiments were performed. There were three proteins that bound to the column loaded with PratA but did not bind to the bare resin. Significant protein hits are defined here as proteins that were present in all three replicates of the pull-down experiments but were absent in the three controls with bare resin.

Protein ID	Description
Q55154.1	Chaperone protein DnaK1
P22358.1	Chaperone protein DnaK2
P73203.3	Phycobilisome linker polypeptide CpcC1

Table 3: Significant proteins bound to PratA from pull-down assays.

Preliminary crystallization:

Efforts to crystallize PratA are ongoing. With the assistance of Dr. Svetlana Pakhomova, we have identified several promising conditions, but no large protein crystals have been prepared to date.

3.3 Discussion:

A PratA plasmid was constructed and the sequence was verified with DNA sequencing. PratA was heterologously expressed in *E. coli* as a His_6-Bla-PratA fusion protein. The expressed protein was cleaved with TEV protease and purified using nickel-affinity chromatography. The presence of PratA was confirmed with SDS-PAGE.

Preliminary binding experiments indicated that no PratA bound to the spinach PSII membranes. In the control PSII lanes, no PratA is present. In the apo-OEC-PSII lanes, PsbO (33 kDa), PsbP (24 kDa), and PsbQ (17 kDa) are all absent. In both the control PSII membranes and the extrinsics-depleted membranes, no PratA was shown to bind after analysis by SDS-PAGE. Further analysis by Western blot of binding assay samples indicated that no PratA was bound unless PratA was present in extremely high concentration. This led to the conclusion that PratA does not bind to native PSII, whether the extrinsic subunit proteins are present are not. This is different from the data obtained previously by Klinkert et al. These groups, however, were using yeast two-hybrid experiments while the experiments described here were done using native PSII from spinach. Furthermore, this data may show that PratA does not bind D1. However, we note that PratA is a cyanobacterial protein and these tests were done on PSII isolated from spinach. The preliminary hypothesis was rejected at this point and pull-down experiments were performed.

Pull-down experiments were performed using a Ni^{2+}-NTA column. Samples were analyzed using mass spectrometry. Three replicates were performed and between them all, only three significant hits were indicated. Chaperone protein DnaK1, chaperone protein DnaK2, and phycobilisome linker polypeptide CpcC1. DnaK1 and DnaK2 are cyanobacterial homologous of Heat Shock Protein 70 (Hsp70). These chaperones facilitate proper protein folding. In eukaryotes, the C-terminus of Hsp70 has been shown to interact with the basic residues of TPR proteins (Bohne, 2016). This led to the formation of a new hypothesis that PratA recruits protein chaperones to the PDMs to facilitate efficient protein relocation from the plasma membrane to the thylakoid membrane, shown in Figure 16. Nickelsen and coworkers observed a 200 kDa complex associated with PratA. This complex is not altered in the absence of D1 in either size or amount. The group concluded that two different PratA complexes exist that differ in size as well as location (Schottkowski et al., 2009). This observation is consistent with our current hypothesis and raises the question of whether DnaK proteins are included in this complex.

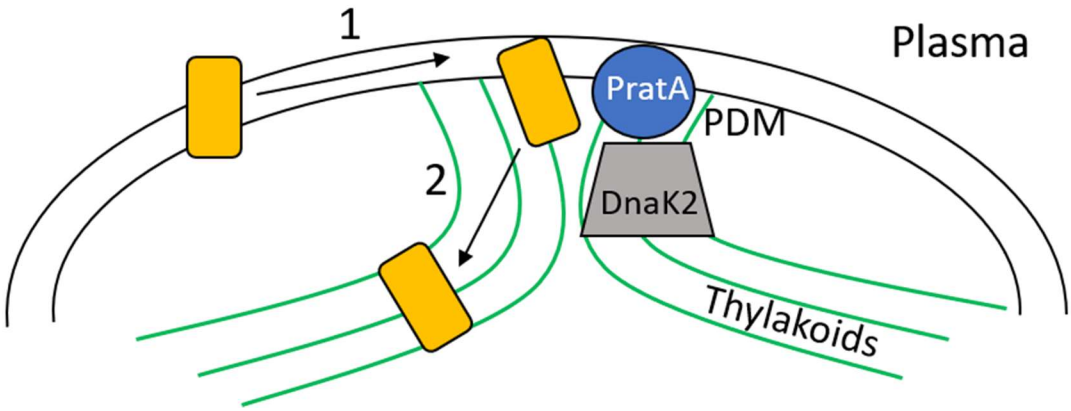

Figure 16: Proposed function of PratA; recruiting protein chaperones to PDMs to facilitate protein relocation between membrane systems. Proteins to be relocated are shown as yellow boxes. Arrow 1 shows the movement of a protein to the PDM where it interacts with PratA and DnaK2. Arrow 2 shows movement of the protein from the PDM to the thylakoids.

Because TPR proteins have been shown to interact with chaperone proteins, this mechanism would provide information on the function of PratA. Transmembrane components of PSII require hydrophobic environments. These components can be found in the thylakoids as well as the plasma membrane, both of which contain different lipid and protein components (Nickelsen et al., 2011). It is important to ensure that proteins do not become denatured or exposed to the cytosol when moving between these different membrane systems. In fact, it has been shown that in cyanobacteria lacking PratA, there was less efficient membrane flow between the plasma membrane and thylakoid membranes (Schottkowski et al., 2009). This type of interaction between protein chaperons and PratA could provide insight into the cyanobacterial mechanism for preventing protein aggregation during protein relocation.

Chapter 4: Conclusions and Future Directions

OEC Depletion:

The two best methods for making OEC-depleted PSII membranes are treatment with $CaCl_2$ and NH_2OH or NaCl and NH_2OH. Treatment with $CaCl_2$ removed all extrinsic subunits, while treatment with NaCl left the extrinsic protein, PsbO. Both methods effectively removed all Mn. Either salt treatment in combination with NH_2OH is efficient for preparing apo-OEC PSII membranes.

Treatment with only NH_2OH did a decent job of depleting the OEC. However, more Mn was present with this preparation method than if the extrinsic subunits had been more fully removed.

The worst method for depleting the OEC was treatment with CHES. This CHES treatment had a similar extrinsic subunit composition as the sample treated with NH_2OH. However, the relative Mn abundance for samples treated with CHES was very high – so high that no photo-assembly experiments were performed.

In the future, binding of PsbO, PsbP, and PsbQ to apo-OEC PSII membranes will be analyzed.

PratA:

PratA has been shown not to bind spinach apo-OEC PSII but has been shown to bind to the chaperone proteins DnaK1 and DnaK2. In ongoing work in the laboratory, both of these cyanobacterial homologs of Heat Shock Protein 70 have been heterologously expressed in *E. coli* with an N-terminal His_6 tag and purified by Ni^{2+} affinity chromatography. The next step is to conduct DnaK-PratA binding experiments. This will be done using pull-down assays and surface plasmon resonance.

Using protocols developed by Nickelsen, plasma membranes, thylakoid membranes, and PDM's have been isolated using ultracentrifugation. Initial experiments have cleanly separated membranes, but the next step is to prevent proteolysis of these samples. These membrane samples will be solubilized, and mass spectrometry will be used to compare protein abundances in each system. These results will test the hypothesis developed from the pull-down assays and may reveal new PratA binding partners.

References

Andersson, B., Critchley, C., Ryrie, I. J., Jansson, C., Larsson, C., & Anderson, J. M. (1984). Modification of the chloride requirement for photosynthetic O_2 evolution. *FEBS Letters*, *168*(1), 113–117. https://doi.org/10.1016/0014-5793(84)80217-3

Baranov, S. V., Tyryshkin, A. M., Katz, D., Dismukes, G. C., Ananyev, G. M., & Klimov, V. V. (2004). Bicarbonate is a native cofactor for assembly of the manganese cluster of the photosynthetic water oxidizing complex. Kinetics of reconstitution of O_2 evolution by photoactivation. *Biochemistry*, *43*(7), 2070–2079. https://doi.org/10.1021/bi034858n

Beck, W. F., de Paula, J. C., & Brudvig, G. W. (1986). Ammonia binds to the manganese site of the O2-evolving complex of Photosystem II in the S_2 State. *Journal of the American Chemical Society*, *108*(14), 4018–4022. https://doi.org/10.1021/ja00274a027

Berthold, D. A., Babcock, G. T., & Yocum, C. F. (1981). A highly resolved, oxygen-evolving photosystem II preparation from spinach thylakoid membranes. EPR and electron-transport properties. *FEBS Letters*, *134*(2), 231–234. https://doi.org/10.1016/0014-5793(81)80608-4

Blankenship, R. E. (2014). *Molecular Mechanisms of Photosynthesis.* Wiley-Blackwell.

Bohne, A. V. (2016). Roles of tetratricopeptide repeat proteins in biogenesis of the photosynthetic apparatus. *International Review of Cell and Molecular Biology*, 187-227. doi:https://doi.org/10.1016/bs.ircmb.2016.01.005

Chen, C., Kazimir, J., & Cheniae, G. M. (1995). Calcium modulates the photoassembly of Photosystem II $(Mn)_4$ -clusters by preventing ligation of nonfunctional high-valency states of manganese. *Biochemistry*, *34*(41), 13511–13526. https://doi.org/10.1021/bi00041a031

Expresso, M. (2015). *Expresso ® Solubility and Expression Screening System*. (January).

Frankel, L. K., & Bricker, T. M. (1995). Interaction of the 33-kDa extrinsic protein with Photosystem II: Identification of domains on the 33-kDa protein that are shielded from NHS-biotinylation by Photosystem II. *Biochemistry*, *34*(22), 7492–7497. https://doi.org/10.1021/bi00022a024

Frankel, L. K., Sallans, L., Bellamy, H., Goettert, J. S., Limbach, P. A., & Bricker, T. M. (2013). Radiolytic mapping of solvent-contact surfaces in Photosystem II of higher plants: Experimental identification of putative water channels within the photosystem. *Journal of Biological Chemistry*, *288*(32), 23565–23572. https://doi.org/10.1074/jbc.M113.487033

Ghanotakis, D. F., & Babcock, G. T. (1983). Hydroxylamine as an inhibitor between Z and P_{680} in Photosystem II. *FEBS Letters*, *153*(1), 231–234. https://doi.org/10.1016/0014-5793(83)80154-9

Ghanotakis, D. F., & Yocum, C. F. (1990). Photosystem II and the oxygen-evolving complex. *Annual Review of Plant Physiology and Plant Molecular Biology*, *41*(1), 255–276. https://doi.org/10.1146/annurev.pp.41.060190.001351

Järvi, S., Suorsa, M., & Aro, E. M. (2015). Photosystem II repair in plant chloroplasts - Regulation, assisting proteins and shared components with Photosystem II biogenesis.

Biochimica et Biophysica Acta - Bioenergetics, *1847*(9), 900–909. https://doi.org/10.1016/j.bbabio.2015.01.006

Klinkert, B., Ossenbühl, F., Sikorski, M., Berry, S., Eichacker, L., & Nickelsen, J. (2004). PratA, a periplasmic tetratricopeptide repeat protein involved in biogenesis of Photosystem II in Synechocystis sp. PCC 6803. *Journal of Biological Chemistry*, *279*(43), 44639–44644. https://doi.org/10.1074/jbc.M405393200

Komenda, J., Sobotka, R., & Nixon, P. J. (2012). Assembling and maintaining the Photosystem II complex in chloroplasts and cyanobacteria. *Current Opinion in Plant Biology*, *15*(3), 245–251. https://doi.org/10.1016/j.pbi.2012.01.017

Miller, A. F., & Brudvig, G. W. (1989). Manganese and calcium requirements for reconstitution of oxygen-evolution activity in manganese-depleted Photosystem II membranes. *Biochemistry*, *28*(20), 8181–8190. https://doi.org/10.1021/bi00446a033

Miyao, M., & Inoue, Y. (1991a). An improved procedure for photoactivation of photosynthetic oxygen evolution: Effect of artificial electron acceptors on the photoactivation yield of NH_2OH-treated wheat Photosystem II membranes. *BBA - Bioenergetics*, *1056*(1), 47–56. https://doi.org/10.1016/S0005-2728(05)80071-4

Miyao, M., & Inoue, Y. (1991b). Enhancement by chloride ions of photoactivation of oxygen evolution in manganese-depleted Photosystem II membranes. *Biochemistry*, *30*(22), 5379–5387. https://doi.org/10.1021/bi00236a008

Nickelsen, J., Rengstl, B., Stengel, A., Schottkowski, M., Soll, J., & Ankele, E. (2011). Biogenesis of the cyanobacterial thylakoid membrane system - an update. *FEMS Microbiology Letters*, *315*(1), 1–5. https://doi.org/10.1111/j.1574-6968.2010.02096.x

Porra, R. J., Thompson, W. A., Kriedemann, P. E. (1989). Determination of accurate extinction coefficients and simultaneous equations for assaying chlorophylls *a* and *b* extracted with four different solvents: verification of the concentration of chlorophyll standards by atomic absorption spectroscopy. *Biochimica et Biophysica Acta*, *975*(2), 389–394.

Radmer, R., & Cheniae, G. M. (1971). Photoactivation of the manganese catalyst of O_2 evolution. II. A two-quantum mechanism. *BBA - Bioenergetics*, *253*(1), 182–186. https://doi.org/10.1016/0005-2728(71)90243-X

Raran-Kurussi S., C. S. (2017). Removal of affinity tags with TEV protease. *Heterologous Gene Expression in E.coli. Methods in Molecular Biology, vol 1586*, 221-230. doi:https://doi.org/10.1007/978-1-4939-6887-9_14

Schottkowski, M., Gkalympoudis, S., Tzekova, N., Stelljes, C., Schünemann, D., Ankele, E., & Nickelsen, J. (2009). Interaction of the periplasmic PratA factor and the PsbA (D1) protein during biogenesis of Photosystem II in *Synechocystis* sp. PCC 6803. *Journal of Biological Chemistry*, *284*(3), 1813–1819. https://doi.org/10.1074/jbc.M806116200

Stengel, A., Gügel, I. L., Hilger, D., Rengstl, B., Jung, H., & Nickelsen, J. (2012). Initial steps of Photosystem II de novo assembly and preloading with manganese take place in biogenesis centers in *Synechocystis*. *Plant Cell*, *24*(2), 660–675. https://doi.org/10.1105/tpc.111.093914

Tamura, N., & Cheniae, G. (1987). Photoactivation of the water-oxidizing complex in Photosystem II membranes depleted of Mn and extrinsic proteins. I. Biochemical and kinetic characterization. *BBA - Bioenergetics*, *890*(2), 179–194. https://doi.org/10.1016/0005-2728(87)90019-3

Vinyard, D. J., Ananyev, G. M., & Charles Dismukes, G. (2013). Photosystem II: The reaction center of oxygenic photosynthesis. *Annual Review of Biochemistry*, *82*(1), 577–606. https://doi.org/10.1146/annurev-biochem-070511-100425

Vinyard, D. J., Badshah, S. L., Riggio, M. R., Kaur, D., Fanguy, A. R., & Gunner, M. R. (2019). Photosystem II oxygen-evolving complex photoassembly displays an inverse H/D solvent isotope effect under chloride-limiting conditions. *Proceedings of the National Academy of Sciences of the United States of America*, *116*(38), 18917–18922. https://doi.org/10.1073/pnas.1910231116

Vinyard, D. J., & Brudvig, G. W. (2017). Progress toward a molecular mechanism of water oxidation in Photosystem II. *Annual Review of Physical Chemistry*, *68*(1), 101–116. https://doi.org/10.1146/annurev-physchem-052516-044820